

Article

# Homoconjugation Mediated Spin-Spin Coupling in Triptycene Nitronyl Nitroxide Diradicals

Chengfang Shi <sup>1</sup>, Laiwei Gao <sup>2</sup>, Martin Baumgarten <sup>3</sup>, Dongdong Wei <sup>2</sup>, Zhipeng Xu <sup>2</sup>, Wenping Wang <sup>1,\*</sup> and Di Wang <sup>2,\*</sup>

<sup>1</sup> School of Chemistry and Chemical Engineering, Hefei University of Technology, Hefei 230009, China  
<sup>2</sup> Anhui Key Laboratory of Advanced Building Materials, School of Materials Science and Chemical Engineering, Anhui Jianzhu University, Hefei 230601, China  
<sup>3</sup> Max Planck Institute for Polymer Research, 55128 Mainz, Germany  
\* Correspondence: wwp65@sina.com (W.W.); wangdi@ahjzu.edu.cn (D.W.)

**Abstract:** In contrast to diradical linked by  $\pi$ -conjugation, there have been only a limited number of studies reported for those linked by homoconjugation systems. Bis(nitronyl nitroxide) diradicals and monoradical connected by a core non-rigid triptycene unit were synthesized. EPR spectroscopy and SQUID were employed to investigate the magnetic exchange interactions. The results demonstrate that the values of  $\Delta E_{ST}$  are 0.19 kcal/mol ( $J = 34.4 \text{ cm}^{-1}$ ) for 2,6-TP-NN and  $-0.21 \text{ kcal/mol}$  ( $J = -36.9 \text{ cm}^{-1}$ ) for 2,7-TP-NN, indicating ferromagnetic interaction and antiferromagnetic interaction, respectively. The spin polarization rule is not a precise predictor of the behavior of triptycene diradicals, and therefore, we improve the model. The experimental findings indicate that homoconjugation can function directly as a coupling pathway between the two spin centers, which is in qualitative agreement with the DFT theoretical calculations and the Borden rule. This research has found a special means of achieving spin coupling in non-rigid aromatics by means of homoconjugation.

**Keywords:** triptycene (TP); nitronyl nitroxide (NN); spin coupling; homoconjugation



**Citation:** Shi, C.; Gao, L.; Baumgarten, M.; Wei, D.; Xu, Z.; Wang, W.; Wang, D.

Homoconjugation Mediated Spin-Spin Coupling in Triptycene Nitronyl Nitroxide Diradicals. *Magnetochemistry* **2023**, *9*, 178. <https://doi.org/10.3390/magnetochemistry9070178>

Academic Editor: Evgenii Moiseevich Pliss

Received: 23 May 2023  
Revised: 29 June 2023  
Accepted: 6 July 2023  
Published: 9 July 2023



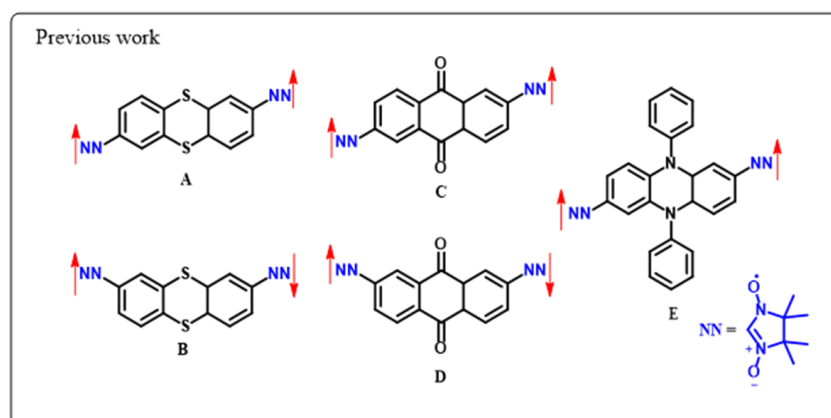
**Copyright:** © 2023 by the authors. Licensee MDPI, Basel, Switzerland. This article is an open access article distributed under the terms and conditions of the Creative Commons Attribution (CC BY) license (<https://creativecommons.org/licenses/by/4.0/>).

## 1. Introduction

Recently, researchers have developed and studied numerous magnetic materials, especially in the realm of organic radicals [1–10]. These materials have a variety of applications, including organic radical-based batteries [4,5], magnetically switched [11–14], magneto-biology [15,16] and magnetic conductivity materials [17–19], in which the magnetic exchange interaction ( $J$ ) between the spin centers plays a critical role in determining the bulk magnetic properties [20]. By tuning the interaction between two spin centers, it is possible to achieve different properties and degrees of coupling of diradicals, typically categorized as intermolecular [21–25] or intramolecular interactions [26,27]. Intermolecular coupling is commonly achieved through H-bonding [21],  $\pi$ -stacking [22–25,28], or other supramolecular interactions [29] between two molecules. Conversely, intramolecular coupling is primarily through chemical bonds [23,30]. The backbone that regulates the coupling of two spin units is called a bridge or coupler, such as  $\pi$ -olefin [31] aromatic conjugation [32,33] and aromatic heterocyclic systems [34]. To date, various diradicals connected by  $\pi$ -conjugated bonds have been extensively studied experimentally and theoretically. The ferromagnetic (FM) interaction and antiferromagnetic (AFM) interaction of these diradicals are readily predicted using the spin polarization [35] or the Borden rule [36,37].

However, predicting intramolecular magnetic exchange interaction for the  $\sigma$ -frame diradical systems [38,39] remains challenging. Examples of conjugated systems containing saturated atoms bridging diradicals have been reported [23,34,40–44]. Izuoka et al. [34] studied the **A** and **B** structures with neutral thianthrene diradicals in Scheme 1 consistent

with the spin polarization of the connecting unit. Akpınar et al. [23] prepared **C** and **D** structures, in addition calculations showed weak ferromagnetic coupling and antiferromagnetic coupling, respectively. Nagata et al. [40] demonstrated that structure **E** possesses a ferromagnetic coupling that can be transformed into an electronic oxide species in the quartet ground state. The first spirocyclic conjugated diradical was synthesized by Frank et al. [41]. Subsequently, Yue et al. [42] investigated three spirobifluorene diradical isomers and further demonstrated that magnetic coupling interaction occurred through spiro conjugation. In 1942, Bartlett et al. [45] firstly synthesized aromatic hydrocarbon triptycene (TP), composed of three benzene rings joined by two  $sp^3$  hybrid carbons. Triptycene has become more popular due to its unique properties [46,47]. Tang et al. [48] synthesized triptycene-bridged tris(thianthrene) compound and discovered cationic main-group triradicals.



**Scheme 1.** Example polycyclic aromatic-linked nitronyl nitroxide diradicals. Two red arrows in the same direction represent FM coupling, and two red arrows in opposite direction represent AFM coupling.

In this study, we prepared 2-TP-NN, 2,6-TP-NN and 2,7-TP-NN by using TP as a coupler to bridge nitronyl nitroxide (NN). The analysis focuses on the magnetic exchange coupling of the triptycene diradicals and the effect of homoconjugation on the overall intramolecular magnetic exchange coupling by linking two spin centers at different substitution positions. Before starting the experiments. We make a tentative qualitative evaluation (Figure 1) of the ground states of 2,6-TP-NN and 2,7-TP-NN and predicted 2,6-TP-NN as a singlet state and 2,7-TP-NN as a triplet state based on the spin polarization rule [35]. On the contrary, the nonbonding molecular orbitals (NBMOs) of 2,6-TP-NN (or 2,7-TP-NN) are expressed as nondisjoint (or disjoint) diradicals (Figure 1), suggesting that 2,6-TP-NN (or 2,7-TP-NN) favors FM coupling (or AFM coupling) via Hund's first rule [37,49]. The two prediction methods give opposite results, which further stimulates our exploration of this topic. UV-visible spectra show that the three radicals NN moieties absorb in the region around 600 nm. Electron paramagnetic resonance (EPR) spectra clearly show different hyperfine splitting between the monoradical and diradicals and indicate that the two diradicals have a certain degree of coupling. Further, superconducting quantum interferometry (SQUID) data indicate that 2,6-TP-NN has a moderate FM coupling with a fitted parameter  $J = 34.4 \text{ cm}^{-1}$ , while 2,7-TP-NN has an AFM coupling with a fitted parameter  $J = -36.9 \text{ cm}^{-1}$ . Density functional theory (DFT) calculations show similar results to the SQUID study, however for the calculated magnetic exchange interaction  $J$  values are relatively small for the diradicals. The above experimental results demonstrate that the "classical" spin polarization rule does not fit triptycene system. So, our study reconsiders the coupling pathway using homoconjugation [50–54] and proposes a special coupling pathway. Apparently, the special pathway fits better with the experimental results as well as the DFT calculations.

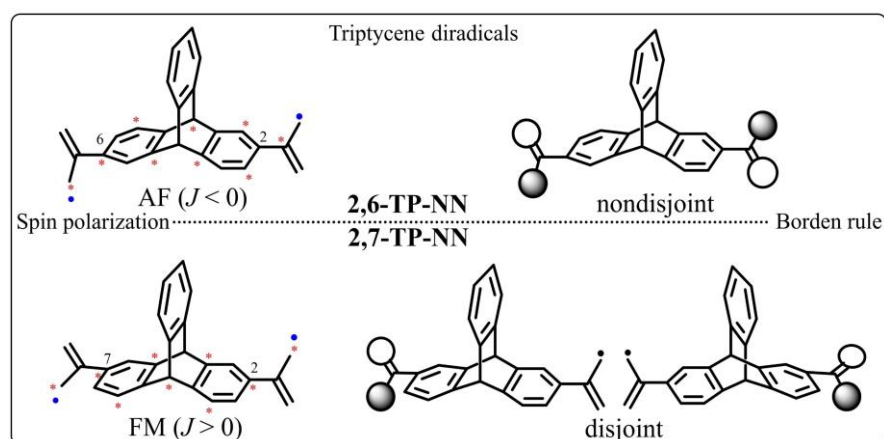
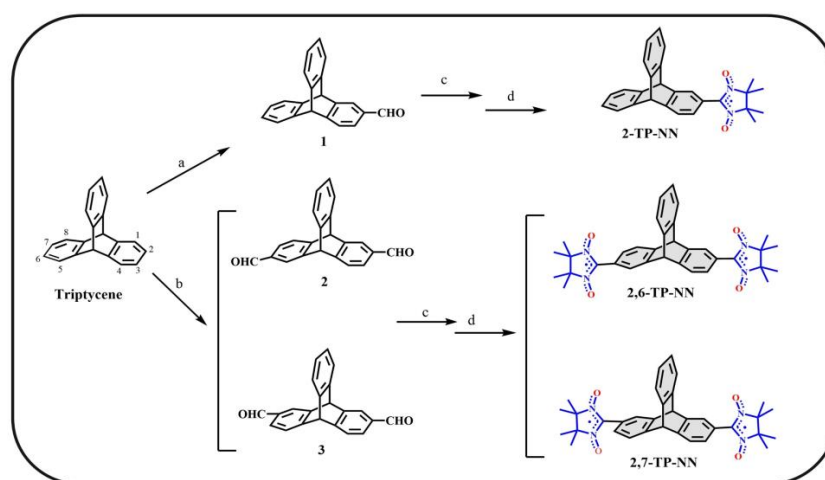


**Figure 1.** Spin prediction model for triptycene diradicals (The red asterisks represent the same spin direction and the dots represent electrons). Preliminary prediction model is that 2,6-TP-NN is antiferromagnetic (AFM) coupling and 2,7-TP-NN is ferromagnetic (FM) coupling.

## 2. Materials and Methods

All radical molecules were synthesized using triptycene as a starting material (see Supplementary Material). The previous literature referred to the preparation of 2,3-bis-(hydroxylamino)-2,3-dimethylbutane (BHA) [55]. 2-Formyltriptycene **1**, as well as diformyltriptycene isomers (**2** and **3**), were prepared from triptycene [56]. The precursors were subjected to Ullman condensation reaction with BHA, resulting in the production of three target products through oxidation (Scheme 2). 2-TP-NN was prepared from triptycene with  $\text{TiCl}_4$  and  $\text{Cl}_2\text{CHOMe}$  in dry  $\text{CH}_2\text{Cl}_2$ , and then condensed with BHA and oxidized by  $\text{NaIO}_4$  to give 2-TP-NN in  $\text{CH}_2\text{Cl}_2/\text{H}_2\text{O}$  at  $0^\circ\text{C}$ . 2-TP-NN appears blue after purification. The precursor diformyltriptycene isomers were prepared by varying the equivalents of  $\text{TiCl}_4$  and  $\text{Cl}_2\text{CHOMe}$ . And after column chromatography to separate regioisomers **2** and **3**, the structural characterization by NMR (Supplementary Material), comparing the chemical shifts ( $\delta = 5.6$  ppm) of the hydrogen spectra of the two isomers, it is clear that **3** results in two  $\text{sp}^3$  hybrid carbon atoms with non-identical proton hydrogen. However, this phenomenon is not present for precursor **2**. The synthetic pathways of 2,6-TP-NN and 2,7-TP-NN are identical to 2-TP-NN (Supplementary Material). The two diradicals also appear as blue powder after purification. Full synthetic details for all target diradicals are provided in the Supplementary Material.



**Scheme 2.** Synthetic routes of the three targeted molecules. (a) 5 eq  $\text{TiCl}_4$ , 5 eq  $\text{Cl}_2\text{CHOMe}$ , DCM; (b) 10 eq  $\text{TiCl}_4$ , 10 eq  $\text{Cl}_2\text{CHOMe}$ , DCM; (c) BHA, DCM/MeOH, reflux, 48 h; (d)  $\text{NaIO}_4$ , DCM/ $\text{H}_2\text{O}$ ,  $0^\circ\text{C}$ .

The single crystal 2-TP-NN was prepared by slowly evaporating in dichloromethane and n-hexane. 2-TP-NN (monoradical), 2,6-TP-NN and 2,7-TP-NN (diradicals) were characterized by UV-vis absorption, electron paramagnetic resonance (EPR), superconducting quantum interferometry (SQUID) and X-ray diffraction. The three radicals were also subjected to density functional theory (DFT) calculations. Additional instrument parameters see the Supplementary Material.

### 3. Results

#### 3.1. Optical Properties

The optical absorption spectra of 2,6-TP-NN and 2,7-TP-NN, together with the  $S = 1/2$  monoradical 2-TP-NN were recorded at room temperature in Figure 2. Absorption is present in some bands for the three radical molecules. Between 250–400 nm, which is the absorption region for  $\pi$ - $\pi^*$  transitions for triptycene moieties, and another weak absorption in the visible region around 500–700 nm, as found for many NN diradicals [22]. All three radical structures have characteristic absorption peaks of NN around 600 nm, mainly caused by the  $n$ - $\pi^*$  transitions of the NN moieties. The UV-vis absorption spectrum strongly indicates that the NN has been synthesized and is absent of imino-nitroxide (IN).

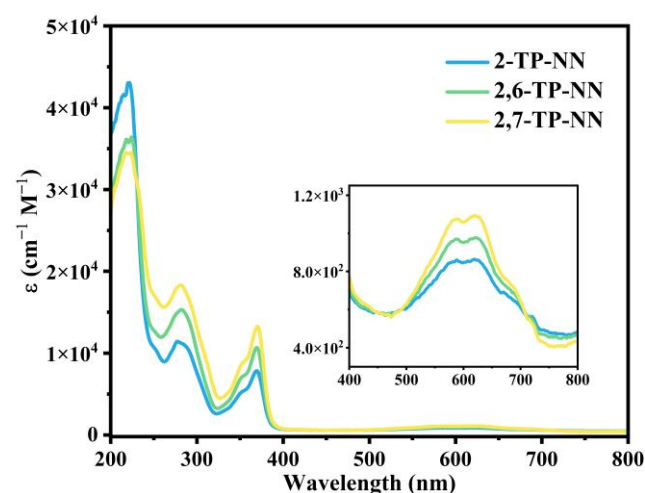


**Figure 2.** UV-vis absorption spectra for 2-TP-NN (blue), 2,6-TP-NN (green) and 2,7-TP-NN (yellow) in toluene ( $\sim 10^{-5}$  M) solution at room temperature. Inset plot: amplification from 400–800 nm.

The experimental data of the three molecules ( $\epsilon$ ,  $\lambda_{\max}$  and optical gap  $E_g$ ) are presented in Table 1. The absorption intensity of 2-TP-NN is weaker near 600 nm (blue) than the other diradicals. The optical gap ( $E_g$ ) of 2,7-TP-NN was determined to be 1.80 eV based on the onset of the  $n$ - $\pi^*$  transition absorption edge, which is larger than the optical gap ( $E_g$ ) of 1.72 eV for 2,6-TP-NN. Figure S1 illustrates the more pronounced differences between the precursor and each of the three radicals.

**Table 1.** Optical and EPR properties with data of the three triptycene radicals.

Radicals	$\lambda_{\max}$ (nm) <sup>1</sup>	$\epsilon$ (cm <sup>-1</sup> M <sup>-1</sup> ) <sup>1</sup>	$E_g^{\text{opt}}$ (eV) <sup>2</sup>	$g$ <sup>3</sup>	$a_{N/2}$ (G) <sup>3</sup>
2-TP-NN	620	866	1.75	2.0065	7.50
2,6-TP-NN	622	974	1.72	2.0063	3.75
2,7-TP-NN	619	1094	1.80	2.0062	3.74

<sup>1</sup> Obtained from UV-vis absorption spectra. <sup>2</sup> Optical energy gaps estimated from the onset of absorption spectra.

<sup>3</sup> Calculated from experimental EPR spectra.

### 3.2. Electron Paramagnetic Resonance Spectroscopy

The EPR spectra of the three radicals were recorded in degassed toluene solution ( $\sim 10^{-4}$  M) at room temperature. 2-TP-NN shows well-resolved five lines with a spacing of 0.75 mT (peak intensities around 1:2:3:2:1), a typical monoradical NN (Figure S2a). Both 2,6-TP-NN and 2,7-TP-NN (Figure 3) are represented by well-resolved nine lines spectra due to splitting by hyperfine coupling deriving from the four equivalent  $^{14}\text{N}$  nuclei (peak intensities around 1:4:10:16:19:16:10:4:1), suggesting delocalization of the electron throughout the entire system. Because of the remarkable intramolecular spin exchange coupling interaction between the two spin centers ( $J \gg a_{\text{N}}$ ), each hyperfine coupling constant (HFC) is also cut in half ( $a_{\text{N}/2} = 0.375$  mT). Despite the rare occurrence of  $\text{sp}^3$  hybrid carbon within the conjugate skeleton [48,57], 2,6-TP-NN and 2,7-TP-NN maintained a strong coupling ( $J \gg a_{\text{N}}$ ) interaction as compared to the spiro conjugation coupling effect [43]. In addition, we also successfully simulated the EPR of the three triptycene radicals at room temperature (Figures 3 and S2a). The more details are found in Table 1.

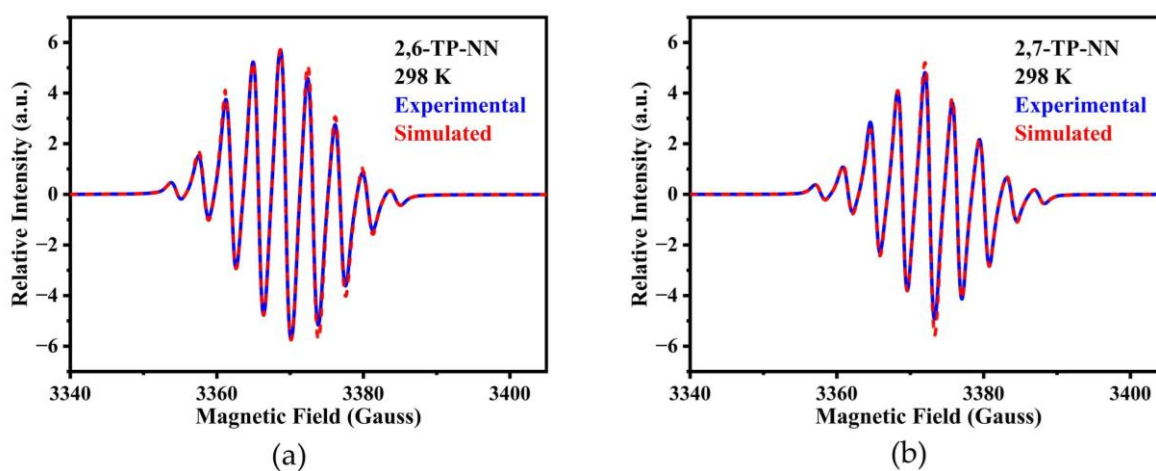


**Figure 3.** EPR spectra in toluene ( $10^{-4}$  M) solution for (a) 2,6-TP-NN and (b) 2,7-TP-NN at room temperature (blue) and simulated (red).

To further understand the internal magnetic coupling of the three triptycene radicals, we performed research tests under low-temperature conditions (100 K, toluene), as illustrated in Figure 4, Figures S2b and S3. We find that both diradicals exhibit strong single peak in the  $g = 2$  region (Figure 4a,b). 2-TP-NN (i.e., monoradical) appears as a regular EPR single peak in this region in line with a simulated spectrum (Figure S2b). The difference between the two diradicals is that 2,6-TP-NN has a sizable main peak with a shoulder, while 2,7-TP-NN has only one main peak, suggesting a smaller zero-field splitting (ZFS) parameter  $D$ . The  $g$  factor of 2,6-TP-NN is anisotropic with  $g_{\text{xx}} = 2.0023$ ,  $g_{\text{yy}} = 2.0078$ ,  $g_{\text{zz}} = 2.0043$  [58]. The zero-field splitting parameters were determined by spectral simulation as  $|D/hc| = 0.00346 \text{ cm}^{-1}$ ,  $|E/hc| = 0.00131 \text{ cm}^{-1}$ . The  $g$  factor of 2,7-TP-NN is anisotropic with  $g_{\text{xx}} = 2.0037$ ,  $g_{\text{yy}} = 2.0042$ ,  $g_{\text{zz}} = 2.0021$ . The slightly smaller the zero-field splitting parameters were determined by spectral simulation as  $|D/hc| = 0.00197 \text{ cm}^{-1}$ ,  $|E/hc| = 0.00048 \text{ cm}^{-1}$ . ZFS phenomenon is caused by dipole-dipole interactions, and the axial system parameter ( $D$ ) is correlated with the distance between the two unpaired electrons ( $r$ ). The average distance between the two spin centers is determined by the point dipole approximation [6,59]. The  $D$  value is affected by the dipole-dipole interactions between the spin units and not directly by the exchange interactions. Furthermore, the  $D$  value is a reflection of the spatial distance between the spin centers. The diradicals 2,6-TP-NN and 2,7-TP-NN correspond to spin centers average distances of 9.09 Å and 10.9 Å, respectively. It is observed that the average distance between 2,6-TP-NN spin centers is slightly smaller than that of 2,7-TP-NN. The results of the DFT calculations

for 2,6-TP-NN (10.7 Å) and 2,7-TP-NN (10.2 Å) were also close to the experimentally measured results.

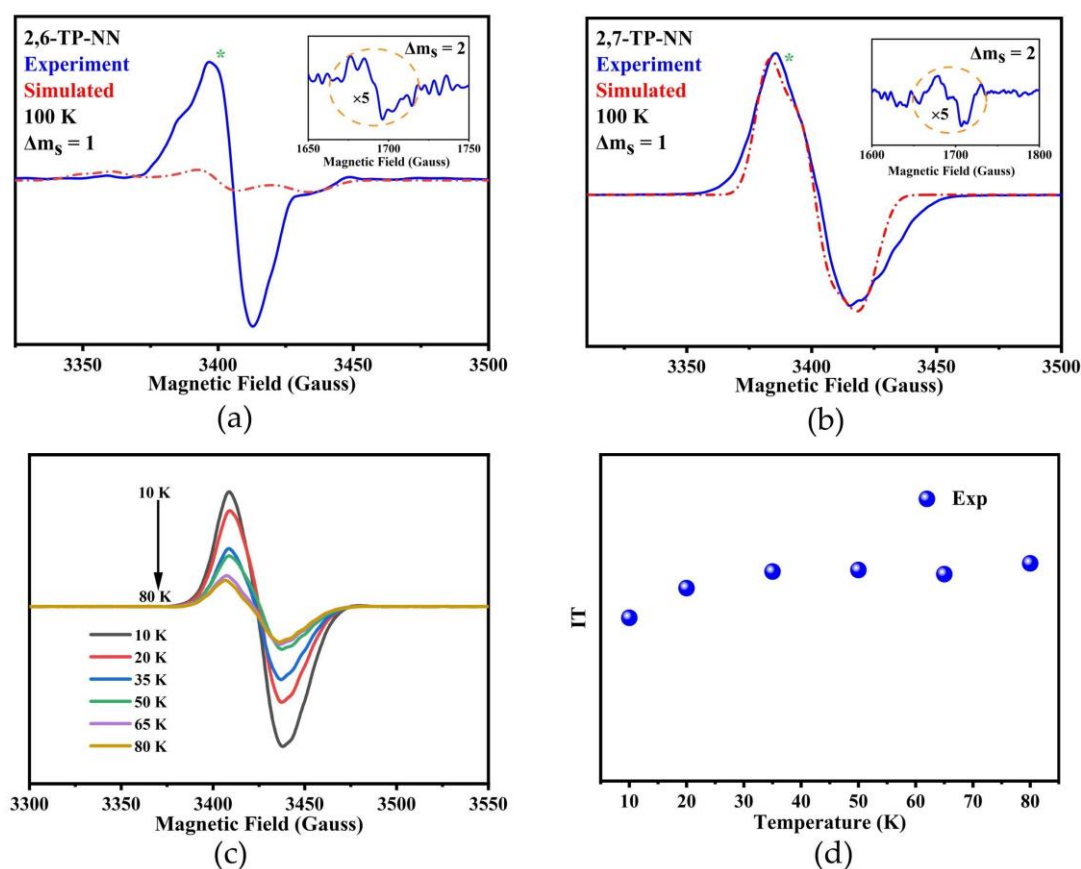


**Figure 4.** Experimental EPR spectra recorded in toluene at 100 K (blue) and simulated (red) of (a) 2,6-TP-NN ( $2D = 74$  G, Fitting results:  $g_{xx} = 2.0023$ ,  $g_{yy} = 2.0078$ ,  $g_{zz} = 2.0043$ ,  $|D/hc| = 0.00346$   $\text{cm}^{-1}$ ,  $|E/hc| = 0.00131$   $\text{cm}^{-1}$ ) and (b) 2,7-TP-NN ( $2D = 42$  G, Fitting results:  $g_{xx} = 2.0037$ ,  $g_{yy} = 2.0042$ ,  $g_{zz} = 2.0021$ ,  $|D/hc| = 0.00197$   $\text{cm}^{-1}$ ,  $|E/hc| = 0.00048$   $\text{cm}^{-1}$ ). The insets show the forbidden transition at half-field (top right). (c) Variable-temperature EPR measurement, 2,7-TP-NN in toluene solution from 10 to 80 K. (d) The measured (solid blue ring) IT-T plot of 2,7-TP-NN. The central peak with a green asterisk shows the signal due to the doublet impurity ( $S = 1/2$ ).

Notably, the weak forbidden transitions ( $|\Delta m_S| = 2$ ) of triplet species were observed in the  $g = 4$  region for 2,6-TP-NN and 2,7-TP-NN (Figure 4a,b inset). The variable-temperature EPR (VT-EPR) experiment was next performed from 10 to 80 K for the diradicals, which showed stronger signal intensities at lower temperatures, indicating the absence of strong antiferromagnetic coupling between the two spin centers (Figures 4c and S4). It is worth noting that the frozen solution spectra of the diradicals both display the EPR signal of the doublet impurity (Figure 4a,b), so the enhancement of the signal at lower temperatures may be contributed by the doublet impurity ( $S = 1/2$ ). Unfortunately, we failed to fit the IT-T plot of the diradicals data with the modified Bleaney-Bowers [60], which is likely to be caused by the presence of the monoradical. The behavior of  $I$  versus  $1/T$  appears to be very close to linear, suggesting the exchange coupling interaction of 2,6-TP-NN and 2,7-TP-NN are relatively weak (Figure S4b,c).

### 3.3. Magnetic Studies

The molar magnetic susceptibility ( $\chi_m$ ) of the three triptycene radical samples were measured using a SQUID magnetometer at temperatures ranging from 2–300 K and at a magnetic field of 1 T, in order to investigate the nature and extent of magnetic exchange

coupling present in the synthesized triptycene radicals. After subtracting the magnetic signal of the empty sample holder, the diamagnetic susceptibility of triptycene was deducted from the Pascal's table [61], and the resulting data are presented in the  $\chi_m$  vs. T curves in the Figure 5. To model the two-spin systems of both diradicals, we employed the Hamiltonian  $H = -2JS_1S_2$  (where  $S_1 = S_2 = 1/2$ ). The experimental data of triptycene diradicals were fitted using the Bleaney-Bowers [62,63] Equation (1).

$$\chi_m T = (1 - F) \frac{2N_A g^2 \mu_B^2}{k_B} \frac{1}{3 + \exp(-2J/k_B T)} \frac{T}{T - \theta} + F \frac{N_A g^2 \mu_B^2}{k_B} \quad (1)$$

where,  $J$  represents the intramolecular exchange of diradicals;  $\theta$  represents the generalized mean field of intermolecular exchange;  $N_A$  represents the Avogadro number,  $g$  represents the isotropic  $g$ -factor,  $k_B$  represents the Boltzmann constant,  $\mu_B$  represents the Bohr magneton and  $F$  represents the paramagnetic impurity.  $J$ ,  $\theta$  and Lande's  $g$  factors are fitted parameters (Tables 2 and S1).

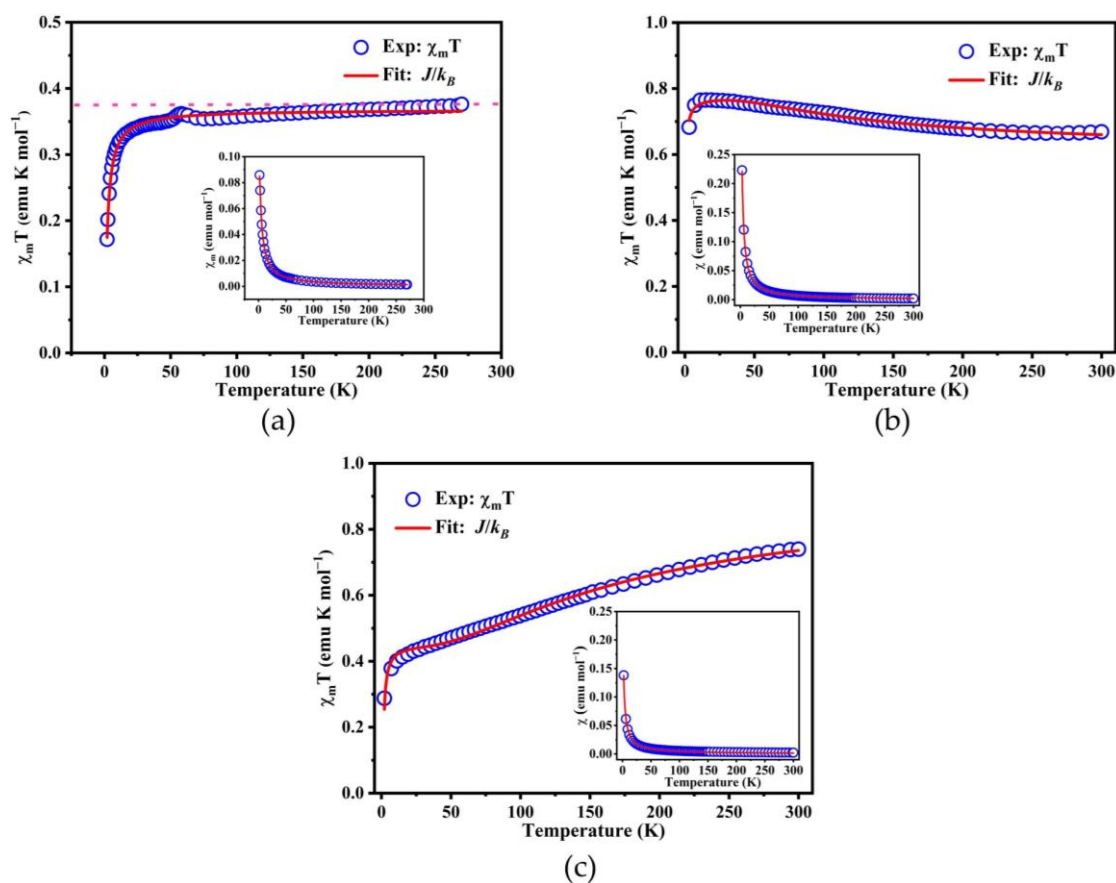


**Figure 5.** SQUID test (blue hollow circle) of the radicals: plots of  $\chi_m T$ -T at a magnetic field of 1 T. Inset plots:  $\chi_m$ -T (blue hollow circle) and fitting (red line) curves of (a) 2-TP-NN, (b) 2,6-TP-NN and (c) 2,7-TP-NN.

**Table 2.** Magnetic Properties of radicals of 2-TP-NN (see Table S1), 2,6-TP-NN and 2,7-TP-NN.

Radicals	$T_{\max}$ (K) <sup>1</sup>	$\theta$ (K)	$J_{\text{exp}}$ (cm <sup>-1</sup> ) <sup>2</sup>	$J_{\text{exp}}$ (cm <sup>-1</sup> ) <sup>3</sup>	$J_{\text{calc}}$ (cm <sup>-1</sup> ) <sup>4</sup>
2,6-TP-NN	14.2	-0.36	-	34.4	1.06
2,7-TP-NN	-	-4.7	-	-36.9	-3.50

<sup>1</sup>  $T_{\max}$  is the temperature corresponding to when  $\chi_m T$  is at the maximum. <sup>2</sup>  $J_{\text{exp}}$  was estimated by fitting IT-T curve from VT-EPR. <sup>3</sup> Estimated from SQUID. <sup>4</sup> Calculated at the UBLYP/6-31G level of DFT.

Figure 5a shows the  $\chi_m T$ - $T$  curve for the monoradical. The  $\chi_m T$  value is  $0.37 \text{ emu K mol}^{-1}$  at 270 K, consistent with the theoretical value of  $0.375 \text{ emu K mol}^{-1}$ . In lower temperature,  $\chi_m T$  decreases rapidly, indicating the presence of antiferromagnetic interaction. For the diradicals, the  $\chi_m T$  values of 2,6-TP-NN (Figure 5b) and 2,7-TP-NN (Figure 5c) were found to be  $0.68 \text{ emu K mol}^{-1}$  and  $0.72 \text{ emu K mol}^{-1}$  at 300 K, respectively. The values are lower than expected value ( $0.75 \text{ emu K mol}^{-1}$ ) for a magnetically independent  $S = 1/2$  two spin units, which may be attributed to additional nonmagnetic material in power sample, with the presence of  $\sim 13\%$  and  $\sim 4\%$  of a nonmagnetic impurity. With the temperature decreases,  $\chi_m T$  of 2,6-TP-NN gradually increases and reaches the maximum value of  $0.77 \text{ emu K mol}^{-1}$  at 14.2 K. On further lowering the temperature,  $\chi_m T$  abruptly decreases until  $\chi_m T = 0.67 \text{ emu K mol}^{-1}$  at 2.0 K. This suggests that there are at least two kinds of magnetic coupling interactions in 2,6-TP-NN, a much weaker intermolecular antiferromagnetic interaction (AFM) as well as moderate intramolecular ferromagnetic interaction (FM). However,  $\chi_m T$  of 2,7-TP-NN keeps falling as the temperature drops until  $\chi_m T = 0.28 \text{ emu K mol}^{-1}$  at 2 K. The temperature dependence of  $\chi_m T$  was fitted by equation (1), giving  $J_{(2,6\text{-TP-NN})} = 34.4 \text{ cm}^{-1}$  ( $\Delta E_{\text{ST}} = 0.19 \text{ kcal/mol}$ ), consistent with weak FM coupling, giving  $J_{(2,7\text{-TP-NN})} = -36.9 \text{ cm}^{-1}$  ( $\Delta E_{\text{ST}} = -0.21 \text{ kcal/mol}$ ), consistent with weak AFM coupling. Obviously, the behaviors of 2,6-TP-NN and 2,7-TP-NN do not obey the spin polarization rule. The inverse of molar magnetic susceptibility versus temperature curve are shown in Figure S5.

### 3.4. X-ray Crystallography

The arrangement and geometry of the molecules in the lattice have a significant impact on magnetic interactions, making it essential to have a clear understanding of radical crystal molecules. By slowly evaporating hexane into a dichloromethane solution, we were able to obtain a needle-like single crystal of 2-TP-NN for X-ray analysis (Figure 6). Many methods of crystallization were tried only to obtain the diradicals crystals that were not large enough to test. The crystal of 2-TP-NN was found to be in the monoclinic crystal system with the  $P2_1/c$  space group. The 2-TP-NN molecular crystal structure revealed that the benzene ring connected with the NN unit exhibited torsions of  $32.5^\circ$  for  $\text{N1}-\text{C21}-\text{C1}-\text{C2}$  (Figure 6b). Such a large torsion angle can prevent the delocalization of electrons in the benzene ring region, resulting in a small spin population of the benzene ring. Similar phenomena have been studied both theoretically and experimentally [24,64–66].

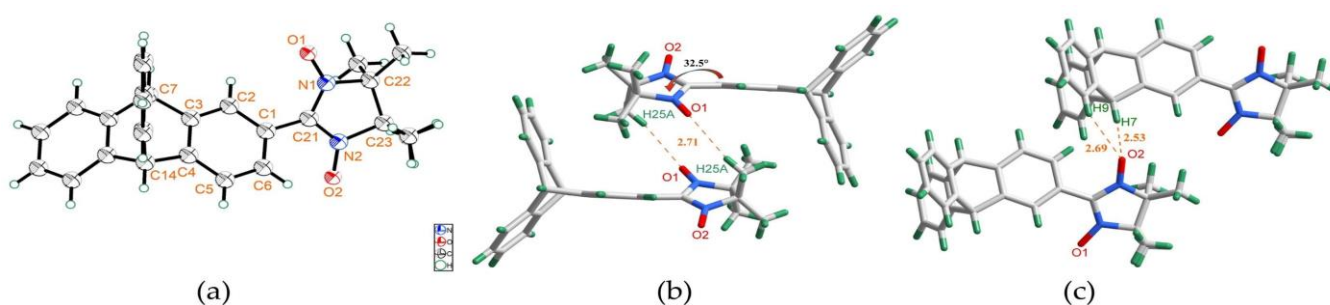


**Figure 6.** Single-crystal structure of 2-TP-NN. (a) ORTEP views, molecular packing along the crystallographic (b) axis a and (c) axis b.

The molecular stacking diagram reveals that 2-TP-NN is arranged vertically along an axis primarily through the NN moieties (Figures 6c and S6c). The oxygen in the NN group forms a short contact distance of  $2.71 \text{ \AA}$  ( $\text{O1}\cdots\text{H25A}$ ) with the adjacent oxygen. Formed dimer is likely to play a role in intermolecular coupling and even in diradicals. The two-dimensional structure shows that the molecules are laterally arranged in a herringbone shape (Figure S6b), with further extension in two dimensions through  $\text{C}-\text{H}\cdots\text{O}$  hydrogen bonds. The oxygen atoms form hydrogen bonds with two hydrogen atoms on the laterally aligned parallel molecule at a distance of  $2.53 \text{ \AA}$  ( $\text{O2}\cdots\text{H7}$ ) and  $2.69 \text{ \AA}$  ( $\text{O2}\cdots\text{H9}$ ), stretching

further in two dimensions through C–H···O hydrogen bonds (Figure S6b). Additional crystallographic data for 2-TP-NN is presented in Tables S2–S4.

### 3.5. Computational Studies

To gain a better understanding of the exchange mechanism in the triptycene radicals, theoretical calculations [66] were performed using Gaussian09 software package. The coupling constants between triptycene diradicals were calculated from the broken-symmetry (BS) by DFT at the UB3LYP/6-31G level of theory, and the computational details are given in the SI. For two exchange coupled unpaired electrons, the simplest Hamiltonian quantity of the molecule is given:  $H = -J_{12}S_1S_2$ . And the magnetic exchange coupling constant ( $J$ ) was calculated according to the following equation proposed by Yamaguchi et al. [67],

$$J = \frac{E_{BS} - E_T}{\langle S^2 \rangle_T - \langle S^2 \rangle_{BS}} \quad (2)$$

where,  $E_{BS}$  and  $E_T$  represent the total energy of the calculated BS singlet state and triplet state,  $\langle S^2 \rangle_T$  and  $\langle S^2 \rangle_{BS}$  represent the total spin angular momentum of the calculated broken-symmetry triplet and singlet state. UB3LYP/6-31G method provides extremely weak positive coupling constant ( $J_{\text{calc}} = 1.06 \text{ cm}^{-1}$ ) and small negative exchange interactions ( $J_{\text{calc}} = -3.50 \text{ cm}^{-1}$ ) for 2,6-TP-NN and 2,7-TP-NN, respectively (Tables 2 and S5), indicating that 2,6-TP-NN has a weak FM coupling, while 2,7-TP-NN has an AFM coupling, in agreement with the experimental results. It is clear that the spin polarization rule is not satisfied for triptycene system, which is likely that  $sp^3$  hybrid carbon atoms break the alternating rule of the coupling path. Such abnormal phenomenon is still observed in the spiro-conjugation system [43].

The spin density distributions of the radicals are shown in Figures 7 and S7. The spin density distributions are mainly delocalized in the NN moieties and the attached benzene rings, while other regions have only small spin densities. The spin population of all heavy atoms within the same phenyl group are added together (Figures 7 and S8). Spin population of diradicals are mainly concentrated in the spin units, with the adjacent benzene ring having only the partial spin population. In addition, the spin population of  $sp^3$  hybrid carbon is almost negligible. Figures 8 and S9 depict the highest single occupied molecular orbitals (SOMOs), visualizing the disjoint and nondisjoint properties of the radicals respectively. The nondisjoint 2,6-TP-NN possesses considerable SOMOs overlap densities and thus have moderate exchange integrals. The calculations reveal that the SOMOs in the diradicals compounds have similar energies (Figures S10 and S11 and Table S6), mainly confined to NN group and exhibiting less domain to the benzene ring. Nevertheless, the disjoint 2,7-TP-NN diradical is distributed in different spatial regions and, as a result, possesses no SOMOs overlap densities, with almost negligible exchange integrals. Consequently, the former prefers triplet state ( $S = 1$ ) and the latter prefers singlet state due to the simplicial SOMOs energy level being broken ( $S = 0$ ).

To further explore the spin coupling within triptycene, we take homoconjugation into account. The influence of the associated  $2p_\pi$ -orbital orientation on magnetic coupling phenomena has also been reported [44]. The  $2p_\pi$ -orbital of the  $sp^2$  carbon atoms adjacent to the methylene may play important role. The spatial distribution of the three benzene rings of triptycene enable the  $sp^2$  carbon atom p-orbitals to overlap partially (Figure 9), which can provide a pathway for intramolecular coupling, although this conjugation effect is small. The through space homoconjugation has been confirmed by many studies [51–53,68,69]. We reconsidered the path for the spin polarization rule, as shown in Figure 9. According to the renew prediction, 2,6-TP-NN exhibits FM coupling, while 2,7-TP-NN presents AFM coupling, which is opposite to previous the spin polarization predictions (Figure 1). The interaction through space is more convincing than the interaction through bond. More importantly, this also provides strong confirmation that the triptycene molecule does contain a special homoconjugation effect.

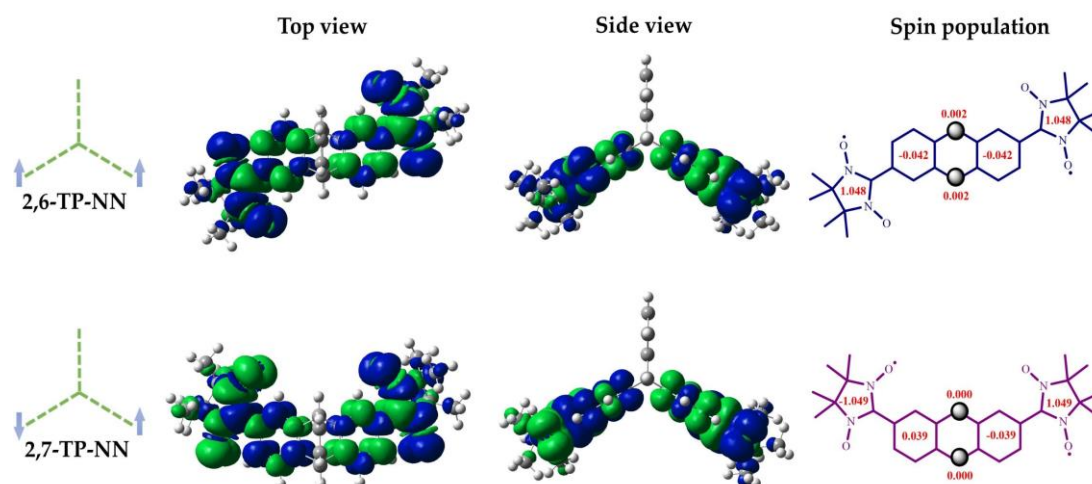


**Figure 7.** Ground state spin density distributions and spin population of 2,6-TP-NN and 2,7-TP-NN (blue and green surfaces represent  $\alpha$  and  $\beta$  spin densities, respectively) calculated at the UB3LYP/6-31G level of theory with an isovalue of 0.004 (The arrows represent the direction).

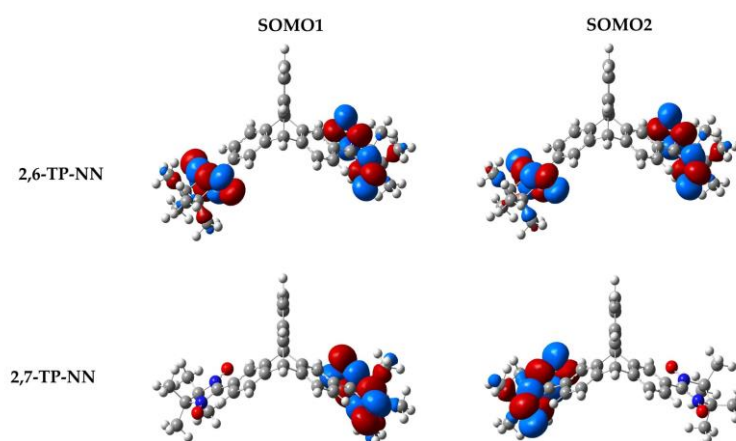


**Figure 8.** Side views SOMOs of 2,6-TP-NN and 2,7-TP-NN (red and blue color represents the different phase of the orbital coefficients), isovalue of 0.004.

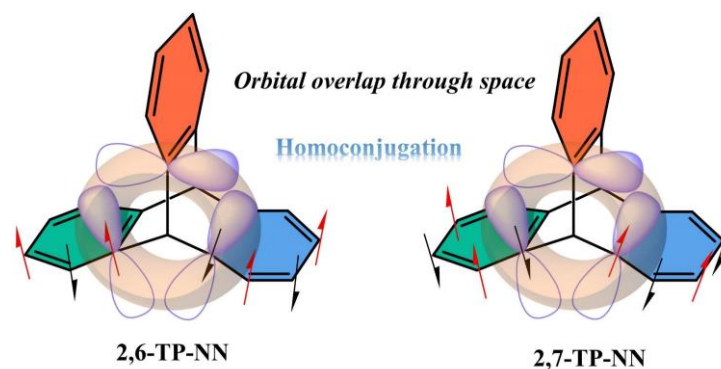


**Figure 9.** Prediction of the spin polarization rule of the triptycene diradicals under homoconjugation (The arrows represent the direction).

#### 4. Conclusions

In summary, three triptycene radicals were synthesized successfully and characterized. The work confirms 2,6-TP-NN with FM coupling as well as 2,7-TP-NN with AFM coupling, consistent with DFT theory. The non-conjugated triptycene system can also provide a pathway for the coupling of spin centers. Unusually, this system did not obey the “classical” spin polarization rule. The coupling pathway does not pass through the  $sp^3$  hybrid carbon atom. To further explain these anomalies, we take the special homoconjugation of triptycene into account, and it was discovered that the unique homoconjugation perfectly accounts for the anomalous prediction by spin polarization. This indicates orbital overlap deriving from the p-orbital of three  $sp^2$  carbon atoms through space can form homoconjugation, making exchange coupling interaction possible. Although the coupling effect of homoconjugation is modest, it provides a new insight into coupling paths for non-conjugation systems, with potential applications in spintronics and molecular electronics.

**Supplementary Materials:** The following supplementary Material can be downloaded at: <https://www.mdpi.com/article/10.3390/magnetochemistry9070178/s1>, Figure S1: Normalized UV–vis absorption spectra of (a) 2-TP-NN, (b) 2,6-TP-NN and (c) 2,7-TP-NN in toluene; Figure S2: EPR spectra in degassed toluene ( $10^{-4}$  M) solution for 2-TP-NN at room temperature (blue) and simulated (red) (a). Experimental EPR spectra recorded in toluene solution for 2-TP-NN at 100 K (blue) and simulated (red) (b); Figure S3: EPR frozen state ZFS spectra for testing, and then rotated  $90^\circ$  for testing of diradicals 2,6-TP-NN (a) and 2,7-TP-NN (b) at 100 K; Figure S4: VT-EPR spectra of (a) 2,6-TP-NN and (b) IT–T plot of 2,6-TP-NN. The observed normalized I–T curve presented as a straight line for (c) 2,6-TP-NN and (d) 2,7-TP-NN; Figure S5: Curie–Weiss model straight line of (a) 2-TP-NN, (b) 2,6-TP-NN and (c) 2,7-TP-NN; Figure S6: Single-crystal structures of 2-TP-NN. (a) The benzene ring connected with NN unit with torsions of  $32.5^\circ$ , (b) The crystal packing of 2-TP-NN along axis b and (c) axis a; Figure S7: Spin density distributions and spin population of 2-TP-NN were calculated using UB3LYP/6-31G method (blue and green surfaces correspond to  $\alpha$  and  $\beta$  spin densities, respectively, with an isovalue of 0.004.); Figure S8: Atomic spin populations calculated using Mullikens protocol at the UB3LYP/6-31G level. (a) 2-TP-NN (b) 2,6-TP-NN (c) 2,7-TP-NN; Figure S9: The 2-TP-NN spatial distribution of molecular orbitals; Figure S10: The 2,6-TP-NN spatial distribution of molecular orbitals; Figure S11: The 2,7-TP-NN spatial distribution of molecular orbitals; Table S1: Magnetic properties of 2-TP-NN. Table S2: Crystal data and structure refinement for 2-TP-NN; Table S3: Bond Lengths for 2-TP-NN; Table S4: Bond Angles for 2-TP-NN; Table S5: Summary of diradical calculation results. Table S6: HOMO, LUMO and HOMO–LUMO ( $\Delta E_{\text{H-L}}$ ) energy. Crystallographic data (CIF); CCDC 2261580 include crystallographic data can be obtained by [https://www.ccdc.cam.ac.uk/data\\_request/cif](https://www.ccdc.cam.ac.uk/data_request/cif) (accessed on 9 May 2023).

**Author Contributions:** Conceptualization, W.W. and D.W. (Di Wang); methodology, C.S. and L.G.; software, C.S., D.W. (Dongdong Wei) and Z.X.; formal analysis, C.S., L.G., D.W. (Dongdong Wei) and Z.X.; investigation, D.W. (Di Wang) and W.W.; resources, D.W. (Di Wang) and W.W.; data curation, C.S., D.W. (Dongdong Wei) and Z.X.; writing—original draft preparation, C.S.; writing—review and editing, C.S., M.B., D.W. (Di Wang) and W.W.; supervision, C.S., D.W. (Di Wang) and W.W.; project administration, D.W. (Di Wang) and W.W.; funding acquisition, D.W. (Di Wang) and W.W. All authors have read and agreed to the published version of the manuscript.

**Funding:** This work was supported by the Natural Science Foundation of China (No. 52003004 and 2013GJMS0526) for the financial support.

**Institutional Review Board Statement:** Not applicable.

**Informed Consent Statement:** Not applicable.

**Data Availability Statement:** Data is available from the corresponding author on reasonable request.

**Acknowledgments:** The authors thank the Max Planck Institute for Polymer Research for providing computing resources. The authors also thank Electron paramagnetic resonance spectroscopy spectra were measured on CIQTEK EPR200-Plus with continuous-wave X band frequency.

**Conflicts of Interest:** The authors declare no conflict of interest.

## References

1. Xu, X.; Takebayashi, S.; Hanayama, H.; Vasylevskiy, S.; Onishi, T.; Ohto, T.; Tada, H.; Narita, A. 6,6'-Biindeno[1,2-b]anthracene: An Open-Shell Biaryl with High Diradical Character. *J. Am. Chem. Soc.* **2023**, *145*, 3891–3896. [[CrossRef](#)] [[PubMed](#)]
2. Shimizu, A.; Morikoshi, T.; Sugisaki, K.; Shiomi, D.; Sato, K.; Takui, T.; Shintani, R. Synthesis and Isolation of a Kekulé Hydrocarbon with a Triplet Ground State. *Angew. Chem. Int. Ed.* **2022**, *61*, e202205729. [[CrossRef](#)]
3. Morita, Y.; Nishida, S.; Murata, T.; Moriguchi, M.; Ueda, A.; Satoh, M.; Arifuku, K.; Sato, K.; Takui, T. Organic tailored batteries materials using stable open-shell molecules with degenerate frontier orbitals. *Nat. Mater.* **2011**, *10*, 947–951. [[CrossRef](#)] [[PubMed](#)]
4. Wang, S.; Easley, A.D.; Lutkenhaus, J.L. 100th Anniversary of Macromolecular Science Viewpoint: Fundamentals for the Future of Macromolecular Nitroxide Radicals. *ACS Macro Lett.* **2020**, *9*, 358–370. [[CrossRef](#)] [[PubMed](#)]
5. Miller, J.S. Magnetically ordered molecule-based materials. *Chem. Soc. Rev.* **2011**, *40*, 3266–3296. [[CrossRef](#)]
6. Abe, M. Diradicals. *Chem. Rev.* **2013**, *113*, 7011–7088. [[CrossRef](#)]
7. Xu, T.; Han, Y.; Shen, Z.; Hou, X.; Jiang, Q.; Zeng, W.; Ng, P.W.; Chi, C. Antiaromatic Dicyclopenta[b,g]/[a,f]naphthalene Isomers Showing an Open-Shell Singlet Ground State with Tunable Diradical Character. *J. Am. Chem. Soc.* **2021**, *143*, 20562–20568. [[CrossRef](#)]
8. Sun, Z.; Ye, Q.; Chi, C.; Wu, J. Low band gap polycyclic hydrocarbons: From closed-shell near infrared dyes and semiconductors to open-shell radicals. *Chem. Soc. Rev.* **2012**, *41*, 7857–7889. [[CrossRef](#)]
9. Ghirri, A.; Candini, A.; Affronte, M. Molecular Spins in the Context of Quantum Technologies. *Magnetochemistry* **2017**, *3*, 12. [[CrossRef](#)]
10. Gertz, I. Likhtenshtein. In *Nitroxides: Brief History, Fundamentals, and Recent Developments*; Springer Nature: Basel, Switzerland, 2020.
11. Paul, A.; Gupta, A.; Konar, S. Magnetic Transition in Organic Radicals: The Crystal Engineering Aspects. *Cryst. Growth Des.* **2021**, *21*, 5473–5489. [[CrossRef](#)]
12. Paul, A.; Nasani, R.; Mondal, A.; Roy, S.; Vela, S.; Konar, S. Reversible Magnetic Transition in a Bench-Stable Radical Cation Triggered by Structural Transition in the Magnetically Silent Counteranion. *Cryst. Growth Des.* **2020**, *20*, 6296–6301. [[CrossRef](#)]
13. Li, T.; Tan, G.; Shao, D.; Li, J.; Zhang, Z.; Song, Y.; Sui, Y.; Chen, S.; Fang, Y.; Wang, X. Magnetic Bistability in a Discrete Organic Radical. *J. Am. Chem. Soc.* **2016**, *138*, 10092–10095. [[CrossRef](#)] [[PubMed](#)]
14. Taponen, A.I.; Ayadi, A.; Lahtinen, M.K.; Oyarzabal, I.; Bonhommeau, S.; Rouzières, M.; Mathonière, C.; Tuononen, H.M.; Clérac, R.; Mailman, A. Room-Temperature Magnetic Bistability in a Salt of Organic Radical Ions. *J. Am. Chem. Soc.* **2021**, *143*, 15912–15917. [[CrossRef](#)]
15. Buchachenko, L. *Magneto-Biology and Medicine*; Nova Science: Hauppauge, NY, USA, 2014.
16. Pierro, A.; Drescher, M. Dance with spins: Site-directed spin labeling coupled to electron paramagnetic resonance spectroscopy directly inside cells. *Chem. Commun.* **2023**, *59*, 1274–1284. [[CrossRef](#)] [[PubMed](#)]
17. Günther, K.; Grabicki, N.; Battistella, B.; Grubert, L.; Dumele, O. An All-Organic Photochemical Magnetic Switch with Bistable Spin States. *J. Am. Chem. Soc.* **2022**, *144*, 8707–8716. [[CrossRef](#)]
18. Ravat, P.; Marszalek, T.; Pisula, W.; Mullen, K.; Baumgarten, M. Positive magneto-LC effect in conjugated spin-bearing hexabenzocoronene. *J. Am. Chem. Soc.* **2014**, *136*, 12860–12863. [[CrossRef](#)]
19. Sugawara, T.; Komatsu, H.; Suzuki, K. Interplay between magnetism and conductivity derived from spin-polarized donor radicals. *Chem. Soc. Rev.* **2011**, *40*, 3105–3118. [[CrossRef](#)]
20. Shimizu, D.; Osuka, A. A Benzene-1,3,5-Triaminy Radical Fused with Zn(II)-Porphyrins: Remarkable Stability and a High-Spin Quartet Ground State. *Angew. Chem. Int. Ed.* **2018**, *57*, 3733–3736. [[CrossRef](#)] [[PubMed](#)]
21. Ravat, P.; Borozdina, Y.; Ito, Y.; Enkelmann, V.; Baumgarten, M. Crystal Engineering of Tolane Bridged Nitronyl Nitroxide Biradicals: Candidates for Quantum Magnets. *Cryst. Growth Des.* **2014**, *14*, 5840–5846. [[CrossRef](#)]
22. Kolanji, K.; Postulka, L.; Wolf, B.; Lang, M.; Schollmeyer, D.; Baumgarten, M. Planar Benzo[1,2-b:4,5-b']dithiophene Derivatives Decorated with Nitronyl and Imino Nitroxides. *J. Org. Chem.* **2019**, *84*, 140–149. [[CrossRef](#)]
23. Akpınar, H.; Schlueter, J.A.; Allão Cassaro, R.A.; Friedman, J.R.; Lahti, P.M. Rigid Core Anthracene and Anthraquinone Linked Nitronyl and Imino Nitroxide Biradicals. *Cryst. Growth Des.* **2016**, *16*, 4051–4059. [[CrossRef](#)]
24. Borozdina, Y.B.; Mostovich, E.; Enkelmann, V.; Wolf, B.; Cong, P.T.; Tutsch, U.; Lang, M.; Baumgarten, M. Interacting networks of purely organic spin-1/2 dimers. *J. Mater. Chem. C* **2014**, *2*, 6618–6629. [[CrossRef](#)]
25. Seber, G.; Freitas, R.S.; Oliveira, N.F.; Lahti, P.M. Crystal Packing and Magnetism in Phenolic Nitronyl Nitroxides: 2-(3',5'-Dimethoxy-4'-hydroxyphenyl)-4,4,5,5-tetramethyl-4,5-dihydro-1H-imidazole-1-oxyl. *Cryst. Growth Des.* **2012**, *13*, 893–900. [[CrossRef](#)]
26. Gaudenzi, R.; de Bruijckere, J.; Reta, D.; Moreira, I.P.R.; Rovira, C.; Veciana, J.; van der Zant, H.S.J.; Burzuri, E. Redox-Induced Gating of the Exchange Interactions in a Single Organic Diradical. *ACS Nano* **2017**, *11*, 5879–5883. [[CrossRef](#)] [[PubMed](#)]
27. Ueda, A.; Nishida, S.; Fukui, K.; Ise, T.; Shiomi, D.; Sato, K.; Takui, T.; Nakasuji, K.; Morita, Y. Three-dimensional intramolecular exchange interaction in a curved and nonalternant  $\pi$ -conjugated system: Corannulene with two phenoxyl radicals. *Angew. Chem. Int. Ed.* **2010**, *49*, 1678–1682. [[CrossRef](#)] [[PubMed](#)]
28. Aboaku, S.; Paduan-Filho, A.; Bindilatti, V.; Oliveira, N.F.; Schlueter, J.A.; Lahti, P.M. Aminophenyl Nitronyl Nitroxides: Highly Networked Hydrogen-Bond Assembly in Organic Radical Materials. *Chem. Mater.* **2011**, *23*, 4844–4856. [[CrossRef](#)]

29. Jiang, W.L.; Peng, Z.; Huang, B.; Zhao, X.L.; Sun, D.; Shi, X.; Yang, H.B. TEMPO Radical-Functionalized Supramolecular Coordination Complexes with Controllable Spin-Spin Interactions. *J. Am. Chem. Soc.* **2021**, *143*, 433–441. [[CrossRef](#)]
30. Ravat, P.; Teki, Y.; Ito, Y.; Gorelik, E.; Baumgarten, M. Breaking the Semi-Quinoid Structure: Spin-Switching from Strongly Coupled Singlet to Polarized Triplet State. *Chem. Eur. J.* **2014**, *20*, 12041–12045. [[CrossRef](#)]
31. Nishide, H.; Kaneko, T.; Nii, T.; Katoh, K.; Tsuchida, E.; Lahti, P.M. Poly(phenylenevinylene)-Attached Phenoxy Radicals: Ferromagnetic Interaction through Planarized and  $\pi$ -Conjugated Skeletons. *J. Am. Chem. Soc.* **1996**, *118*, 9695–9704. [[CrossRef](#)]
32. Haraguchi, M.; Tretyakov, E.; Gritsan, N.; Romanenko, G.; Gorbunov, D.; Bogomyakov, A.; Maryunina, K.; Suzuki, S.; Kozaki, M.; Shiomi, D.; et al. (Azulene-1,3-diyl)-bis(nitronyl nitroxide) and (Azulene-1,3-diyl)-bis(iminonitroxide) and Their Copper Complexes. *Chem. Asian J.* **2017**, *12*, 2929–2941. [[CrossRef](#)]
33. Barker, J.E.; Dressler, J.J.; Cardenas Valdivia, A.; Kishi, R.; Strand, E.T.; Zakharov, L.N.; MacMillan, S.N.; Gomez-Garcia, C.J.; Nakano, M.; Casado, J.; et al. Molecule Isomerism Modulates the Diradical Properties of Stable Singlet Diradicaloids. *J. Am. Chem. Soc.* **2020**, *142*, 1548–1555. [[CrossRef](#)] [[PubMed](#)]
34. Izuoka, A.; Hiraishi, M.; Abe, T.; Sugawara, T.; Sato, K.; Takui, T. Spin Alignment in Singly Oxidized Spin-Polarized Diradical Donor: Thianthrene Bis(nitronyl nitroxide). *J. Am. Chem. Soc.* **2000**, *122*, 3234–3235. [[CrossRef](#)]
35. Kollmar, H.; Staemmler, V. A theoretical study of the structure of cyclobutadiene. *J. Am. Chem. Soc.* **1977**, *99*, 3583–3587. [[CrossRef](#)]
36. Borden, W.T.; Davidson, E.R. Effects of electron repulsion in conjugated hydrocarbon diradicals. *J. Am. Chem. Soc.* **1977**, *99*, 4587–4594. [[CrossRef](#)]
37. Borden, W.T.; Iwamura, H.; Berson, J.A. Violations of Hund's Rule in Non-Kekule Hydrocarbons: Theoretical Prediction and Experimental Verification. *Acc. Chem. Res.* **1994**, *27*, 109–116. [[CrossRef](#)]
38. Suzuki, S.; Itoh, N.; Furuichi, K.; Kozaki, M.; Shiomi, D.; Sato, K.; Takui, T.; Ohi, H.; Itoh, S.; Okada, K. Synthesis and Magnetic Properties of Dimethylmethylenebis(iminonitroxide) Diradical. *Chem. Lett.* **2011**, *40*, 22–24. [[CrossRef](#)]
39. Tsujimoto, H.; Suzuki, S.; Kozaki, M.; Shiomi, D.; Sato, K.; Takui, T.; Okada, K. Synthesis and Magnetic Properties of (Pyrrolidin-1-oxyl)-(Nitronyl Nitroxide)/(Iminonitroxide)-Dyads. *Chem. Asian J.* **2019**, *14*, 1801–1806. [[CrossRef](#)]
40. Nagata, A.; Hiraoka, S.; Suzuki, S.; Kozaki, M.; Shiomi, D.; Sato, K.; Takui, T.; Tanaka, R.; Okada, K. Redox-Induced Modulation of Exchange Interaction in a High-Spin Ground-State Diradical/Triradical System. *Chem. Eur. J.* **2020**, *26*, 3166–3172. [[CrossRef](#)]
41. Natia, L.F.; Rodolphe, C.; Jean-Pascal, S.; Nathalie, D.; Olivier, K.; Claude, C.; Green, M.T.; Stéphane, G.; Lahcène, O. Synthesis, Crystal Structure, Magnetic, and Electron Paramagnetic Resonance Properties of a Spiroconjugated Biradical. Evidence for Spiroconjugation Exchange Pathway. *J. Am. Chem. Soc.* **2000**, *122*, 2053–2061. [[CrossRef](#)]
42. Yue, Z.; Liu, J.; Baumgarten, M.; Wang, D. Spirobifluorene Mediating the Spin-Spin Coupling of Nitronyl Nitroxide Diradicals. *J. Phys. Chem. A* **2023**, *127*, 1565–1575. [[CrossRef](#)]
43. Kanetomo, T.; Ichihashi, K.; Enomoto, M.; Ishida, T. Ground Triplet Spirobiradical: 2,2',7,7'-Tetra(tert-butyl)-9,9'(10 H,10' H)-spirobiacridine-10,10'-dioxyl. *Org. Lett.* **2019**, *21*, 3909–3912. [[CrossRef](#)] [[PubMed](#)]
44. Rajca, A.; Mukherjee, S.; Pink, M.; Rajca, S. Exchange coupling mediated through-bonds and through-space in conformationally constrained polyradical scaffolds: Calix[4]arene nitroxide tetradicals and diradical. *J. Am. Chem. Soc.* **2006**, *128*, 13497–13507. [[CrossRef](#)] [[PubMed](#)]
45. Bartlett, P.D.; Ryan, M.J.; Cohen, S.G. Triptycene<sup>1</sup> (9,10-o-Benzoanthracene). *J. Am. Chem. Soc.* **1942**, *64*, 2649–2653. [[CrossRef](#)]
46. Jiang, Y.; Chen, C.F. Recent Developments in Synthesis and Applications of Triptycene and Pentiptycene Derivatives. *Eur. J. Org. Chem.* **2011**, *2011*, 6377–6403. [[CrossRef](#)]
47. Wozny, M.; Mames, A.; Ratajczyk, T. Triptycene Derivatives: From Their Synthesis to Their Unique Properties. *Molecules* **2021**, *27*, 250. [[CrossRef](#)]
48. Tang, S.; Ruan, H.; Hu, Z.; Zhao, Y.; Song, Y.; Wang, X. A cationic sulfur-hydrocarbon triradical with an excited quartet state. *Chem. Commun.* **2022**, *58*, 1986–1989. [[CrossRef](#)]
49. Tretyakov, E.V.; Zhivetyeva, S.I.; Petunin, P.V.; Gorbunov, D.E.; Gritsan, N.P.; Bagryanskaya, I.Y.; Bogomyakov, A.S.; Postnikov, P.S.; Kazantsev, M.S.; Trusova, M.E.; et al. Ferromagnetically Coupled S=1 Chains in Crystals of Verdazyl-Nitronyl Nitroxide Diradicals. *Angew. Chem. Int. Ed.* **2020**, *59*, 20704–20710. [[CrossRef](#)]
50. Ferguson, L.N.; Nnadi, J.C. Electronic interactions between nonconjugated groups. *J. Chem. Educ.* **1965**, *42*, 529. [[CrossRef](#)]
51. Harada, N.; Uda, H.; Nakasuji, K.; Murata, I. Interchromophoric homoconjugation effect and intramolecular charge-transfer transition of the triptycene system containing a tetracyanoquinodimethane chromophore. *J. Chem. Soc. Perkin Trans.* **1989**, *21*, 1449–1453. [[CrossRef](#)]
52. Kobayashi, T.; Kubota, T.; Ezumi, K. Intramolecular orbital interactions in triptycene studied by photoelectron spectroscopy. *J. Am. Chem. Soc.* **2002**, *105*, 2172–2174. [[CrossRef](#)]
53. Perevedentsev, A.; Francisco-López, A.; Shi, X.; Braendle, A.; Caseri, W.R.; Goñi, A.R.; Campoy-Quiles, M. Homoconjugation in Light-Emitting Poly(phenylene methylene): Origin and Pressure-Enhanced Photoluminescence. *Macromolecules* **2020**, *53*, 7519–7527. [[CrossRef](#)]
54. Baumgärtner, K.; Hoffmann, M.; Rominger, F.; Elbert, S.M.; Drew, A.; Mastalerz, M. Homoconjugation and Intramolecular Charge Transfer in Extended Aromatic Triptycenes with Different  $\pi$ -Planes. *J. Org. Chem.* **2020**, *85*, 15256–15272. [[CrossRef](#)]
55. Wang, D.; Ma, Y.; Wolf, B.; Kokorin, A.I.; Baumgarten, M. Temperature-Dependent Intramolecular Spin Coupling Interactions of a Flexible Bridged Nitronyl Nitroxide Biradical in Solution. *J. Phys. Chem. A* **2018**, *122*, 574–581. [[CrossRef](#)]

56. Li, P.F.; Chen, C.F. Synthesis, structures, and solid state self-assemblies of formyl and acetyl substituted triptycenes and their derivatives. *J. Org. Chem.* **2012**, *77*, 9250–9259. [[CrossRef](#)] [[PubMed](#)]
57. Zoppellaro, G.; Geies, A.; Andersson, K.K.; Enkelmann, V.; Baumgarten, M. Synthesis, Optical Properties and Magnetic Studies of 2,6-Bis(pyrazolylmethyl)pyridine Functionalized with Two Nitronyl Nitroxide Radicals. *Eur. J. Org. Chem.* **2008**, *2008*, 1431–1440. [[CrossRef](#)]
58. Stoll, S.; Schweiger, A. EasySpin, a comprehensive software package for spectral simulation and analysis in EPR. *J. Magn. Reson.* **2006**, *178*, 42–55. [[CrossRef](#)]
59. Mukai, K.; Sakamoto, J. Spin–spin dipolar and exchange interactions in crystalline bisgalvinoxyl biradical. *J. Chem. Phys.* **1978**, *68*, 1432–1438. [[CrossRef](#)]
60. Hase, S.; Shiomi, D.; Sato, K.; Takui, T. Phenol-substituted nitronyl nitroxide biradicals with a triplet ( $S = 1$ ) ground state. *J. Mater. Chem. C* **2001**, *11*, 756–760. [[CrossRef](#)]
61. Bain, G.A.; Berry, J.F. Diamagnetic Corrections and Pascal’s Constants. *J. Chem. Educ.* **2008**, *85*, 532. [[CrossRef](#)]
62. Bleaney, B.; Bowers, K. Anomalous paramagnetism of copper acetate. *Proc. R. Soc. London Ser. A* **1952**, *214*, 451–465. [[CrossRef](#)]
63. Han, H.; Zhang, D.; Zhu, Z.; Wei, R.; Xiao, X.; Wang, X.; Liu, Y.; Ma, Y.; Zhao, D. Aromatic Stacking Mediated Spin–Spin Coupling in Cyclophane-Assembled Diradicals. *J. Am. Chem. Soc.* **2021**, *143*, 17690–17700. [[CrossRef](#)]
64. Malik, R.; Bu, Y. Intramolecular Proton Transfer Modulation of Magnetic Spin Coupling Interaction in Photochromic Azobenzene Derivatives with an Ortho-Site Hydroxyl as a Modulator. *J. Phys. Chem. A* **2022**, *126*, 9165–9177. [[CrossRef](#)] [[PubMed](#)]
65. Borozdina, Y.B.; Mostovich, E.A.; Cong, P.T.; Postulka, L.; Wolf, B.; Lang, M.; Baumgarten, M. Spin-dimer networks: Engineering tools to adjust the magnetic interactions in biradicals. *J. Mater. Chem. C* **2017**, *5*, 9053–9065. [[CrossRef](#)]
66. Bajaj, A.; Ali, M.E. First-Principle Design of Blatter’s Diradicals with Strong Ferromagnetic Exchange Interactions. *J. Phys. Chem. C* **2019**, *123*, 15186–15194. [[CrossRef](#)]
67. Yamaguchi, K.; Jensen, F.; Dorigo, A.; Houk, K.N. A spin correction procedure for unrestricted Hartree-Fock and Møller-Plesset wavefunctions for singlet diradicals and polyradicals. *Chem. Phys. Lett* **1988**, *149*, 537–542. [[CrossRef](#)]
68. Haselbach, E.; Neuhaus, L.; Johnson, R.P.; Houk, K.N.; Paddon-Row, M.N.  $\pi$ -Orbital Interactions in Möbius-Type Molecules as Studied by Photoelectron Spectroscopy. *Helv. Chim. Acta* **1982**, *65*, 1743–1751. [[CrossRef](#)]
69. Chen, Z.; Swager, T.M. Synthesis and Characterization of Poly(2,6-triptycene). *Macromolecules* **2008**, *41*, 6880–6885. [[CrossRef](#)]

**Disclaimer/Publisher’s Note:** The statements, opinions and data contained in all publications are solely those of the individual author(s) and contributor(s) and not of MDPI and/or the editor(s). MDPI and/or the editor(s) disclaim responsibility for any injury to people or property resulting from any ideas, methods, instructions or products referred to in the content.